EVALUATING THE EFFECT OF LARGE AND SPREAD EXPLOSIVES LOADS

Bibiana M. Luccioni[a,c], Daniel Ambrosini[b,c], Steeve Chung Kim Yuen[d] and Gerald N. Nurick[d]

[a]*Instituto de Estructuras, Universidad Nacional de Tucumán, Av. Roca 1800, 4000 S.M. de Tucumán , Argentina, blucciont@herrera.unt.edu.ar.edu.ar, www.herrera.unt.edu.ar/iest*

[b] *Facultad de Ingeniería, Universidad Nacional de Cuyo, Centro Universitario - Parque Gral. San Martín - 5500 Mendoza, dambrosini@uncu.edu.ar , http://fing.uncu.edu.ar/*

[c]*CONICET, Av Rivadavia 1917, Cdad de Bs As*

[d] *Blast Impact and Survivability Research Unit (BISRU), Department of Mechanical Engineering, University of Cape Town, Private Bag, Rondebosch 7701, South Africa, www.bisru.uct.ac.za*

Keywords Explosion, soil, blast wave, crater, damage, numerical model.

Abstract. Reports on experiments or numerical analysis involving medium to extreme explosive devices (> 100 kg TNT) are scarce. Blast wavefront parameters and scaling laws found in the specialized literature have usually been obtained and used for spherical explosive charges. Similarly, empirical equations proposed for the evaluation of crater dimensions produced by explosions on the ground level were obtained for compact charges that is spherical or cylindrical charges, and explosive masses up to 100 kg of TNT.

This paper presents the numerical analysis of the detonation of explosive charges ranging from 1000 to 26,288 kg of TNT laid on the ground, mainly widespread in a carpet-like form. The charges consist of different ordnances stacked in different configurations. The effects of the charge configurations and mass of explosive on the crater dimensions and blast wave parameters are investigated. While the cube root scaled distance works well for a relatively compact charge layout the scaled distance parameter has to be modified for cases where charges are spread in a carpet-like form. Numerical results are compared with experimental results of crater dimensions and blast wave parameters. Reasonable agreement with the experiments is obtained.

1   INTRODUCTION

Explosive devices are available in different sizes. Table 1 lists the suggested classification for explosive devices, in four main groupings based on the size of the charge, by Nurick et al. (2006). Category S1 is a device of mass up to 0.1 kg of TNT that enables indoor laboratory blast testing. Category S2 (0.1-10 kg TNT) consists of devices that require outdoor laboratory experimentation. The explosive devices in the medium (M: 10-100 kg TNT), large (L: 100-1000kg TNT) and extreme (E: >1000kg TNT) categories consist of different size weapon-type systems. See Table 1.

Category	SMALL		MEDIUM	LARGE	EXTREME
	S1	S2	M	L	E
Facilities	Indoor Laboratory	Outdoor Laboratory /Test Range	Test Range	Test Range	Test Range
Mass	Up to 0.1 Kg	>0.1 Kg to 10Kg	>10 Kg to 100Kg	>100Kg to 1000Kg	>1000Kg
Example	Hand grenade Antipersonnel Mine	Land-Mine Portable Mines	Torpedo Air Bomb	War Head	Oklahoma Nuclear bomb
References	Telling-Smith and Nurick (1991); Nurick and Shave (1996) Nurick and Martin (1989a); Nurick and Martin (1989b)	Guruprasad and Mukherjee (2000); Jacinto et al (2001); Hanssen et al (2002)	Formby and Wharton (1996); Wharton et al (2000)		Lok (2005); Hirschfelder et al. (1945)

Table 1: Categorization of size of explosive devices.

Whilst numerous different tests investigating the response of structures, such as beams and plates, to blast loading conditions in the S1 category have been published in the open literature, reports describing structural response using medium to extreme explosive devices are scarce (Chung Kim Yuen et al., 2008).

Empirical equations for the evaluation of blast wave parameters can be found in the specialized literature. These equations have been, however, obtained for spherical explosives of less than 1000 kg of TNT. Moreover, these formulas are based on scaling laws that were proved to work well for that shape of explosives. There are also several studies related to blast load assessment and the effect of blast loads for spherical explosives of no more than 1000 kg of TNT on structures (Luccioni et al., 2006). Recently a study investigating craters created by exploding charges ranging from 120 kg to 1900 kg of TNT was presented (Ambrosini and Luccioni, 2008). The charge consists of different ordnances stacked in different configurations corresponding to tests performed at Touwsrivier Training Range (South Africa) (Chung Kim Yuen et al., 2008). The arrangement of the explosive load was shown to have significant importance in the final dimensions of the crater.

This paper presents the numerical analysis of blast tests in the extreme category (masses of

explosive greater than 1000 kg of TNT). The test programme was performed at the Vastrap Weapons Range, South Africa (Chung Kim Yuen et al., 2008). The charge consists of different ordnances widespread in a carpet-like form. Numerical results are compared with experimental results of crater dimensions and blast wave parameters. The effects of the charge configurations and mass of explosive on the crater dimensions and blast wave parameters are investigated.

2   EXPERIMENTAL PROGRAM (Chung Kim Yuen et al., 2008)

The tests were conducted on the Vastrap Weapons Range located 1000 km north west of Cape Town, a vast test area, which is a fairly flat and sandy. Because of its vast area each test was carried out on a different location on the range leaving the crater resulting from the blast untouched. 11 blast tests—ranging from 500 to 26,288 kg of TNT were performed. The list of ordnance used to make up the charge load is listed in Table 2. The blasts were created using ordnance such as Projectile AS MK 10, Warhead KC5, Warhead KC9, 84mm HE and 90mm HE shells. Each test comprised a stack of ammunition as required to configure the predetermined mass. The ordnance was laid out in a carpet-like way on the flat ground in different stacking pattern to provide the most favourable packing –labour –time layout. A typical charge lay-out is shown in Fig. 1(a) (Test 10).
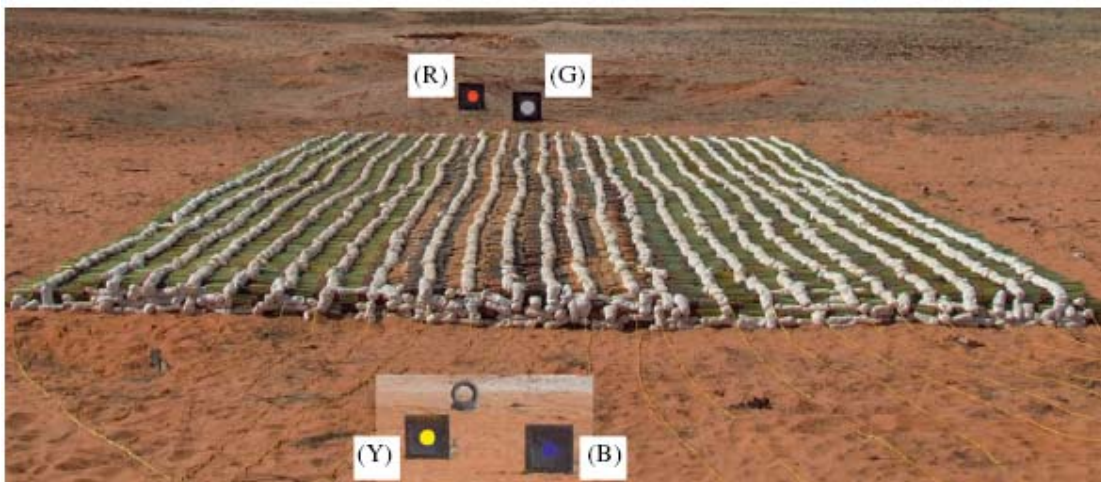
a)
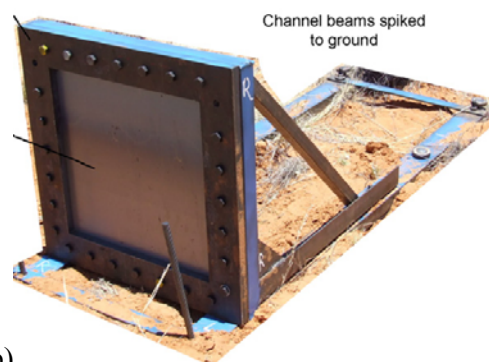
b)

Figure 1: Blast test 10. a) Explosive layout; b) Steel plate

Blast	Explos. Mass W kg TNT	Plate thickness h (mm)	Stand off distance R (m)	Measured deflection δ (mm)	Crater dimensions (m)		
					a	b	H_2
1	1119.8	6	18.50	0.0	8.7	10.8	0.8
		3	18.00	5.0			
		3	22.50	2.5			
		3	19.50	4.2			
2	1135.2	6	8.80	14.7	----	----	----
		3	13.35	28.6			
		3	12.25	37.3			
		3	8.65	40.7			
3	2250.6	3	13.30	35.5	10.3	12.0	0.9
		3	15.00	33.1			
		6	11.30	37.3			
		3	18.60	22.0			
4	3694.8	3	18.20	36.8	10.7	18.7	1.8
		6	16.20	18.1			
		3	27.90	12.8			
		3	20.70	34.7			
5	6945.4	6	21.25	0.0	11.0	23.0	2.2
		3	24.65	7.4			
		3	25.45	0.0			
		3	20.95	7.9			
6	3395.6	3	21.00	9.1	17.0	22.2	2.3
		6	14.50	45.2			
		3	18.00	35.5			
		3	16.00	50.2			
7	13222	6	19.30	4.2	15.3	21.6	----
		3	27.20	15.7			
		3	22.85	10.4			
		3	19.20	27.8			
8	22054.9	3	26.60	34.8	15.0	25.5	2.7
		3	24.90	31.8			
		3	20.20	60.6			
9	600	3	14.80	23.0	8.1	8.1	2.5
10	27569.3	6	17.00	70.2	20.2	27.2	3.0
		3	20.80	103.0			
		3	24.00	50.9			
		3	20.40	202.0			
11	27223.6	6	22.30	70.3	-----	-----	-----
		3	25.50	83.0			

Table 2: Vastrap tests (Chung Kim Yuen et al., 2008)

For almost all the tests the dimensions of the craters produced by the explosive loads were measured as indicated in Fig.2 and presented in Table 2. Three or four (grey (G), red (R), blue (B), yellow(Y)) quadrangular mild steel plates of 3 and 6mm thick were placed at different distances from the explosives loads and were subjected to pressure loads generated by the blast. A plate-clamping station, 700x700 mm^2 in size, shown in Fig 1(b), was used to provide the quadrangular specimen with suitable support to enable the pressure loadings to result in large inelastic deformations of the exposed area of 500 x 500 mm^2. The mid point deflections of all the plates were recorded and listed in Table 2.
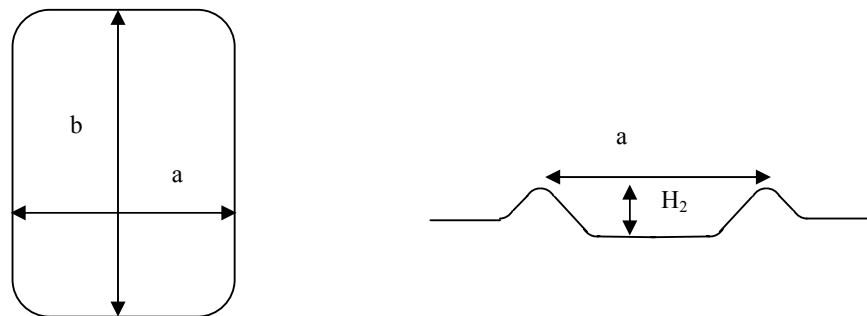
Figure 2: Crater sketch

3   EMPIRICAL EQUATIONS

3.1 Introduction

Historically, the analysis of explosions either has predominantly involved simplified analytical methods (Baker et al., 1983; Kinney and Graham, 1985; Smith and Hetherington, 1994). Nowadays empirical formulas are still obtained from numerical and experimental studies are very useful to perform quick prediction of the response of soils and structures to blast load. A brief description of the empirical formulas that are later compared with experimental and numerical results of blast wave parameters, plate deflections and craters dimensions are presented in this section.

3.2 Blast wave parameters

When a condensed high explosive is detonated, a blast wave is formed. It is characterized by an abrupt pressure increase at the shock front, followed by a quasi-exponential decay back to ambient pressure and a negative phase in which the pressure is less than environmental pressure.

The most widely used approach for blast wave scaling is Hopkinson's law (Baker et al., 1983) which establishes that similar explosive waves are produced at identical scaled distances when two different charges of the same explosive and with the same geometry are detonated in the same atmosphere. Thus, any distance R from an explosive charge W can be transformed into a characteristic scaled distance Z,

$$Z = R/W^{1/3} \tag{1}$$

where W is the charge mass expressed in kilograms of TNT. The use of Z allows a compact and efficient representation of blast wave data for a wide range of situations. There are many solutions for the wave front parameters from both numerical solution and experimental measurements (Baker et al., 1983; Kinney and Graham, 1985; Smith and Hetherington, 1994). The results are usually presented in graphics, tables or equations based on experimental or numerical results, such as the following equations,

$$\frac{P_s}{P_o} = \frac{808\left[1 + (Z/4.5)^2\right]}{\sqrt{1 + (Z/0.048)^2}\sqrt{1 + (Z/0.32)^2}\sqrt{1 + (Z/1.35)^2}} \tag{2}$$

Where P_s is the peak overpressure and P_o is the atmospheric pressure.

It is important to note that Eq.(2) and most empirical formula found in the specialized literature are based on the assumption that the blast originates from a spherical charge. Moreover, the accuracy of predictions and measurements in the near field is lower than in the far field, probably due to the complexity of blast phenomena (Smith and Hetherington, 1994).

3.3 Determination of the mid-point deflection

Dimensionless analysis provides a useful insight into scaling to enable a better understanding of the characteristic response of geometrically similar plates subjected to impulsive loading. Nurick and Martin (1989a; b) presented an empirical relationship to predict the mid-point deflection–thickness ratio of thin quadrangular plates subjected to uniform blast load. From this relationship, the mid-point deflection of a 500x500 mm2 and 3mm thick steel plate (static yield stress=250MPa, density=7850 kg/m3) can be calculated (Chung Kim Yuen et al. 2008) as

$$\delta[\text{mm}] = 0.114I \text{ [N s]} \tag{3}$$

where I is the total impulse on the plate that can be approximated as

$$I = i_s A \tag{4}$$

where A is the exposed area of the plate and i_s the specific impulse.

3.4 Crater formation

A crater is always formed when an explosive load is detonated on the soil surface. The crater dimensions defined by Kinney and Graham (1985) are used in this work (Figure 3): D is the apparent crater diameter, D_r is the actual crater diameter and H_2 is the apparent depth of the crater.
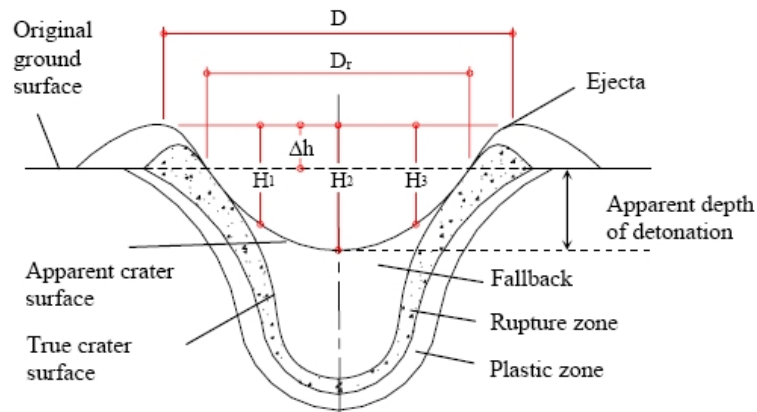
Figure 3: Definitions of the crater dimensions.

Studies concerned with the characteristics of craters caused by explosions usually resort to dimensional analysis and statistics. The scaling law establishes that any linear dimension L of the crater can be expressed as a constant multiplied by W^α divided by the distance of the charge from the ground, where α is a coefficient that is dependent on whether the gravitational effects can be neglected or not. When the gravitational effects can be neglected the cubic root law is applicable α =0.33 and in the other cases the functional dependence can be quite complex.

There is not much information about explosions at ground level. Statistical studies of about 200 accidental above-ground explosions of relatively large magnitude are presented by Kinney and Graham (1985). The results exhibit a variation coefficient in the crater diameter of about 30%. From these results, the following empirical equation for the crater diameter was proposed (Kinney and Graham, 1985)

$$D(m) = 0.8W^{1/3}(kg) \pm 30\% \qquad (5)$$

The authors have conducted a series of tests performed with different amounts of explosive at short distances above and below ground level, as well as on the soil surface (Ambrosini et al., 2002). They also presented (Ambrosini and Luccioni, 2006) a numerical study on craters formed by explosive loads located on the soil surface. From these results, the following equation has been proposed for the evaluation of the apparent diameter of the crater formed by spherical blast loads laid on the ground,

$$D(m) = 0.51W^{1/3}(kg) \pm 5\% \qquad (6)$$

The variation of ±5% accounts for the differences between soil properties that could be found in different sites.

4   NUMERICAL MODELS

4.1 Introduction

All the numerical analysis is performed with a hydrocode (AUTODYN v11.0, 2007). In order to carry out a comparable analysis, the mass of the explosive is defined by TNT masses. The corresponding masses for other explosives can be obtained through the concept of TNT

equivalence (Formby, 1996).

An Euler Godunov multi material with strength higher order processor (Alia and Souli, 2006) is used to model the problems including the air, the explosive charge and the soil.

4.2 Material models

4.2.1 Air

The ideal gas equation of state is used for the air. In an ideal gas, the internal energy is a function of the temperature alone and if the gas is polytropic the internal energy is simply proportional to temperature. It follows that the equation of state for a gas, which has uniform initial conditions, may be written as,

$$p = (\gamma - 1)\rho e \tag{7}$$

in which p is the hydrostatic pressure, ρ is the density and e is the specific internal energy. γ is the adiabatic exponent, it is a constant (equal to $1 + R/cv$) where constant R may be taken to be the universal gas constant R_0 divided by the effective molecular weight of the particular gas and cv is the specific heat at constant volume. The values of the constants used for air are presented in Table 3.

Equation of State: Ideal gas
$\gamma = 1.4$
Reference density: $\rho_a = 1.225 \ 10^{-3}$ g/cm^3
Reference temperature: $T_o = 288.2$ K
Specific heat: $c_v = 717.3$ J/kgK

Table 3: Air properties

4.2.2. TNT

Lee-Tarver equation of state (Lee and Tarver, 1980) is used to model both the detonation and expansion of TNT in conjunction with "Jones - Wilkins - Lee" (JWL EOS) to model the unreacted explosive.

The (JWL) equation of state can be written as,

$$p = C_1\left(1 - \frac{\omega}{r_1 v}\right)e^{-r_1 v} + C_2\left(1 - \frac{\omega}{r_2 v}\right)e^{-r_2 v} + \frac{\omega e}{v} \tag{8}$$

Where p is the hydrostatic pressure, $v = 1/\rho$ is the specific volume, ρ is the density, C1, r1, C2, r2 and ω (adiabatic constant) are constants and their values have been determined from dynamic experiments and are available in the literature for many common explosives. The values used for TNT are presented in Table 4.

$$
\boxed{
\begin{array}{l}
\text{Equation of State: JWL} \\[4pt]
\text{Reference density } \rho = 1.658 \text{ g/cm}^3 \\[4pt]
C_1 = 3.7377 \ 10^8 \text{ kPa} \\[4pt]
C_2 = 3.73471 \ 10^6 \text{ kPa} \\[4pt]
R_1 = 4.15 \\[4pt]
R_2 = 0.9 \\[4pt]
\omega = 0.35 \\[4pt]
\text{C-J detonation velocity: } 6.93 \ 10^3 \text{ m/s} \\[4pt]
\text{C-J energy/unit volumen: } 6 \ 10^6 \text{ KJ/m}^3 \\[4pt]
\text{C-J pressure: } 2.1 \ 10^7 \text{ kPa}
\end{array}
}
$$

Table 4: TNT properties

4.2.3. Soil

A shock equation of state combined with an elastoplastic strength model based on Drucker Prager criterion and a hydro tensile limit are used for the soil. The initial density is taken as ρ = 2.2 g/cm3 (wet density). The wet density is obtained considering a mean dry density of 2100 kg/m3 and a moisture content of 5%.

The experimental fact is that for most solids and many liquids, that do not undergo a phase change, the values on the shock Hugoniot for shock velocity U and material velocity behind the shock up can be adequately fitted to a straight line

$$U = c_o + su_p \tag{9}$$

Where c_0 is sound speed.

The Mie-Gruneisen form of equation of state based on the shock Hugoniot is used:

$$p = p_h + \Gamma \rho (e - e_h) \tag{10}$$

Where Γ is the Gruneisen Gamma G, defined as:

$$\Gamma = v \left(\frac{\partial p}{\partial v} \right)_v \tag{11}$$

It is assumed that $\Gamma \rho = \Gamma_0 \rho_0 = constant$ and

$$p_h = \frac{\rho_o c_o^2 \mu (1+\mu)}{\left[1-(s-1)\mu\right]^2} \quad e_h = \frac{1}{2}\frac{p_h}{p_o}\left(\frac{\mu}{1+\mu}\right) \tag{12}$$

The assumption of constant $\Gamma\rho$ is probably not valid. Furthermore, the assumption of a linear variation between the shock velocity U and the particle velocity u_p does not hold for too large a compression. At high shock strengths some nonlinearity in this relationship is apparent, particularly for non-metallic materials. This non linearity is covered by a smooth interpolation between two linear relationships.

A Drucker Prager criterion with standard values is adopted for the strength model. The yield stress is a piecewise linear function of pressure.

A summary of soil properties used for soil is presented in Table 5.

Equation of State: Shock	Strength: Drucker Prager
Reference density ρ = 2.2 g/cm^3	
Gruneisen Gamma Γ = 0.11	
c_o = 1.614 10^3 m/s	
S =1.5	
Shear Modulus G = 2.4 10^5 kPa	
Pressure 1 =-1.149 10^3 kPa	Yield stress 1 = 0 kPa
Pressure 2 = 6.88 10^3 kPa	Yield stress 2 = 6.2 10^3 kPa
Pressure 3 = 1.0 10^{10} kPa	Yield stress 3 = 6.2 10^3 kPa
Hydro tensile limit p_{min} = -100 kPa	

Table 5: Soil properties

4.3 Boundary conditions

In order to fulfill the radiation condition, a transmitting boundary is defined for soil subgrids external limits. The transmit boundary condition allows a stress wave to continue "through" the physical boundary of the subgrid without reflection. The size of the numerical mesh can be reduced using this type of boundary condition. The transmit boundary is only active for flow out of a grid. The effectiveness of this boundary condition is checked in some of the examples presented in this paper.

5   CRATER FORMATION

5.1 Introduction

The simulation of craters produced by explosive loads widespread in a carpet-like form is presented in this section. First three blast tests described in section 2 are numerically reproduced and the results are compared with experimental ones. Once the ability of the

numerical model has been checked, further numerical analysis is carried out in order to study the effects of the charge configurations and mass of explosive on the crater dimensions.

5.2 Numerical simulation of Vapstrap tests

Three typical tests covering the range of 1119.8-27569.3 kg TNT were numerically simulated. These tests correspond to blast tests 1, 5 and 10 in Table 2. In order to carry out a comparable analysis, the mass of the explosive is defined by TNT masses. Using symmetry conditions, only a quarter of the problem was simulated. The numerical models used are presented in Fig. 4. In each model soil, air and TNT were modeled. For clarity air is not represented in the models shown in Fig.4. The explosive was widespread in the same area as in the experiment. In the case of test 1, three explosive strips were modeled to represent the experiments. The mesh was refined in coincidence with the explosive load. Detonation lines were defined in correspondence with detonators in each test. The simulation was carried out until the craters remain unchanged.

Fig.5 shows the craters produced by the explosive tests and those obtained with the numerical models. The experimental and numerical results for the crater dimensions are presented in Table 6. There is a reasonable agreement between numerical and experimental results. The differences are in the order of the variability in experimental measures for this type of tests. The craters simulated are always smaller and more stretched than actual craters and a good agreement in crater depth indicated as H_2 in Fig. 3 is achieved.

Tests	Results	a(m)	b(m)	b/a	H_2(m)
Blast 1	Exper.	8.7	10.8	1.2	0.8
1119.8 kg	Numer.	6.3	10.6	1.7	0.7
TNT	Difer. %	28%	1.6%	--	16%
Blast 5	Exper.	11	23	2.09	2.2
6945.4 kg	Numer.	8.2	22.6	2.75	2.5
TNT	Difer. %	25%	1.7%	--	-13.6%
Blast 10	Exper.	20.2	27.2	1.34	3
27569.3 kg	Numer.	15.76	23	1.45	3.30
TNT	Difer.%	21,9%	15.4		-10%

Table 6: Crater dimensions

a)

b)

c)
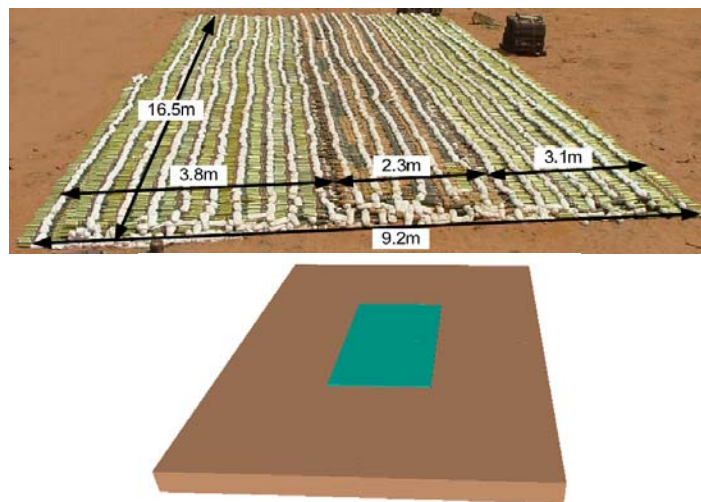
Figure 4: Numerical models for Vastrap tests. a) Test 1 (1119.8 kg TNT); b) Test 5 (6945.4 kg TNT); c) Test 10 (27569.3 kg TNT)

a)
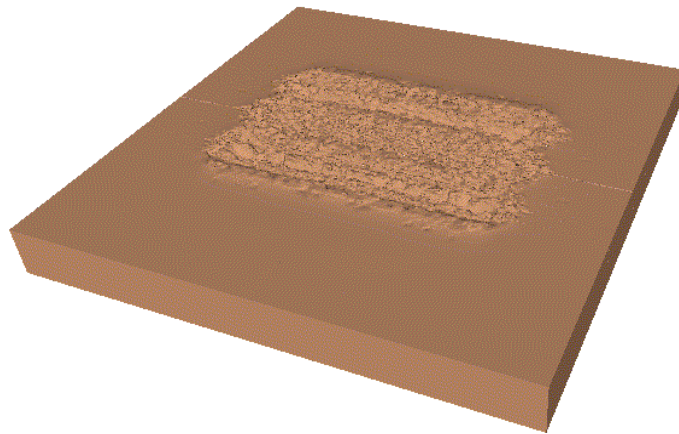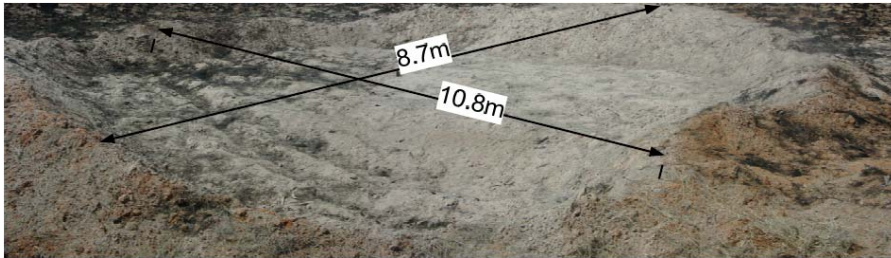
b)
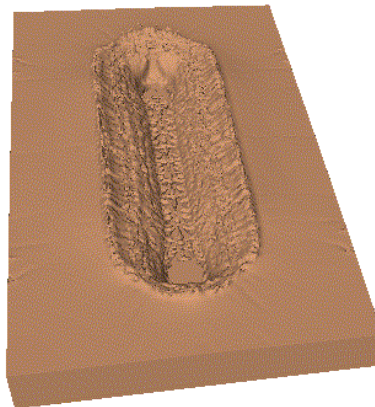
c)
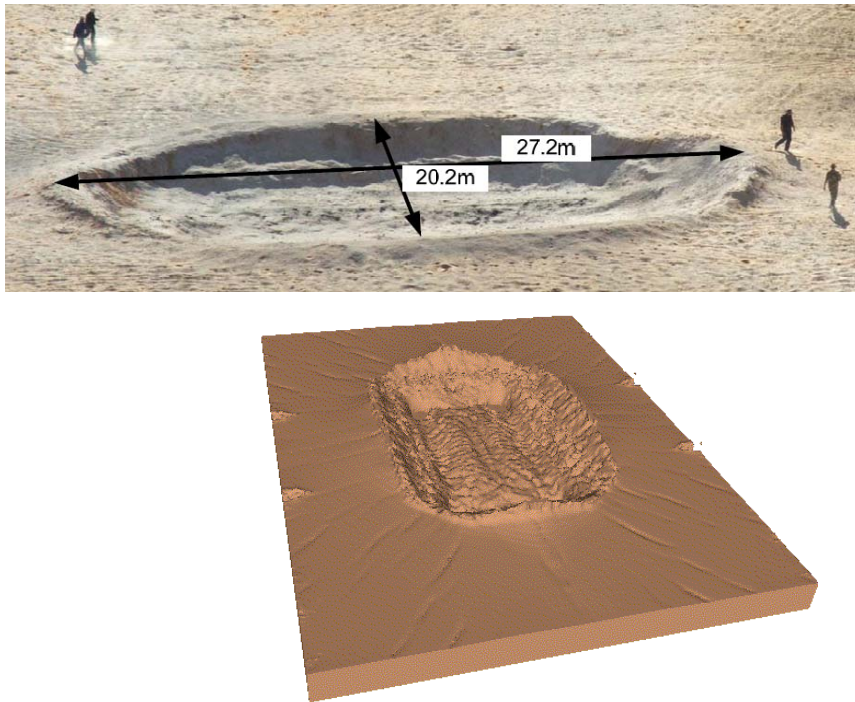
Figure 5: Experimental and numerical craters for Vastrap tests. a) Test 1 (1119.8 kg TNT); b) Test 5 (6945.4 kg TNT); c) Test 10 (27569.3 kg TNT)

5.3 Craters produced by axial symmetric blast loads

In order to study the effect of explosive charge layout on crater dimensions, the craters produced by the same explosive charges but with cylindrical shape were simulated. Two different layouts were modeled for each explosive mass: (C) a cylindrical carpet like layout with the same area in plan than the tests and (M) a cylindrical compact layout with diameter equal to height. Typical models for both cases are shown in Fig.6. The dimensions of the explosive cylinders used for each test are presented in Table 7. Due to symmetry conditions, these problems were simulated with axial symmetric models with a considerable save in computer time in comparison with actual shape numerical tests presented in section 5.2.

a)   b)
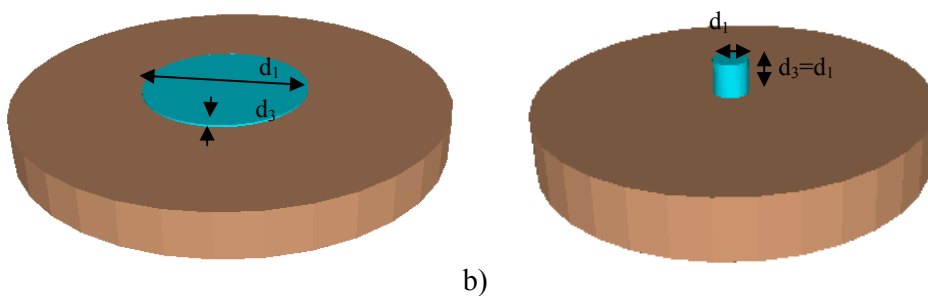
Figure 6: Numerical models for axial symmetric numerical tests (6945.4 kg TNT). a) Carpet like explosive (C); b) Compact layout (M)

W (kg TNT)	Carpet like explosive layout (C)		Compact explosive (M)
	d_1 (mm)	d_3 (mm)	d_1 (mm)= d_3 (mm)
1119.8	7440	15.8	814.1
6945.4	7720	91	1757
27569.3	13930	11.1	2780

Table 7: Explosive dimensions for axial symmetric numerical tests

The craters numerically obtained for 1119.8 kg TNT with both (C) and (M) explosive layouts are shown in Fig.7. The diameters of the carters are presented in Table 8 for comparison with experimental and numerical equivalent diameter (diameter of the circle with equal area) of the craters produced by actual shape explosives. It can be seen that the equivalent diameter of craters produced by cylindrical explosive loads is always smaller than that obtained for the rectangular layout used in the tests. Moreover, when the explosive is concentrated in a compact cylinder (M), even smaller craters are obtained.

W (kg TNT)	Rectangular layout Equivalent crater diameter D (m)		Cylindrical layout Crater diameter D (m)	
	Exper.	Numer.	Numer - Carpet like explosive (C)	Numer.-Compact explosive (M)
1119.8	10.9	9.2	8.4	6.0
6945.4	17.9	15.4	11.8	8.5
27569.3	26.4	21.5	18.4	11.1

Table 8: Crater diameters for axial symmetric numerical tests

a)

b)
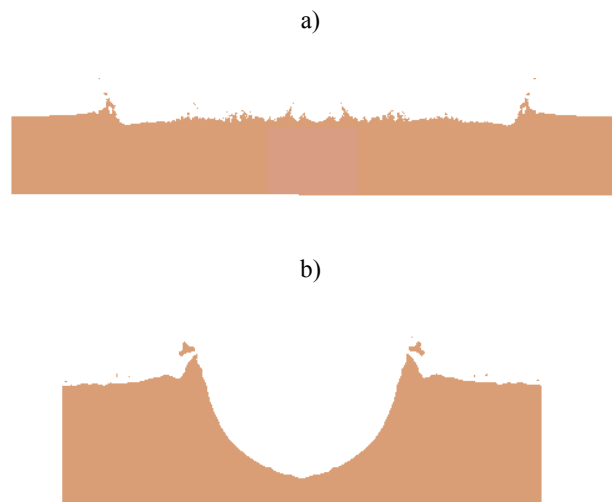
Figure 7: Craters obtained for axial symmetic numerical tests (1119.8 kg TNT). a) Carpet like explosive (C); b) Compact layout (M)

5.4 Analysis of results

All the results obtained in previous sections are plotted on Fig.8 representing the equivalent apparent crater diameter as a function of the cubic root of the equivalent TNT explosive mass for comparison. The lines representing Eqs. (5) and (6) together with points corresponding to experimental and numerical results previously obtained by the authors are also plotted in Fig.8. The points correspond to experimental results from crater tests with spherical explosive loads of 1-10 kg TNT lying on the ground (Ambrosini et al. 2002), numerical crater tests with spherical explosive loads of 50-500 kg TNT lying on the ground (Ambrosini and Luccioni 2006) and numerical crater tests for compact (not cylindrical) explosive charge layouts of 120-1900 kg TNT reported by Ambrosini and Luccioni (2008).
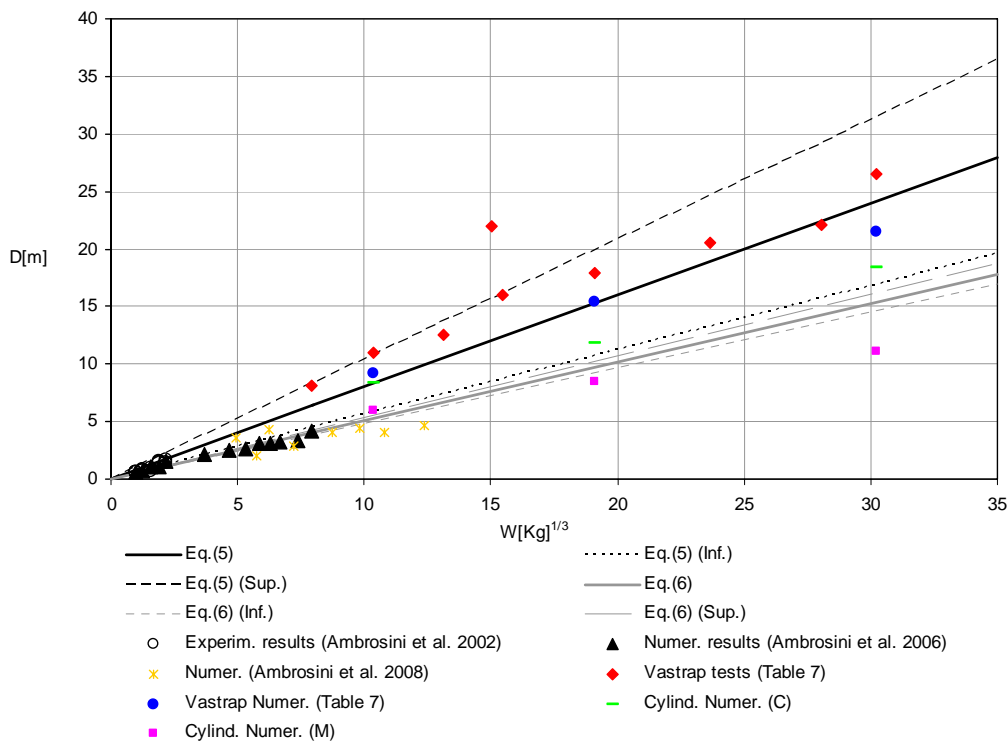
Figure 8: Apparent crater diameter for explosive load on the ground

The tendency remarked in previous section relating craters produced by different explosive layouts is clear in Fig.8. While craters produced by carpet like explosives are better represented by Eq.(5), crater diameters obtained for compact explosives are better represented by Eq.(6). In both cases, it seems that the linear approximation is only valid for explosive loads up to the large category (L) (less than 1000 kg TNT). In order to represent the complete range of explosive masses simulated, the following equations are proposed and represented in Fig.9 together with experimental and numerical results.

$$(C) \qquad D(m) = 1.7463 W^{1/4} \tag{13}$$

$$(M) \qquad D(m) = 0.8338 W^{1/4} \tag{14}$$
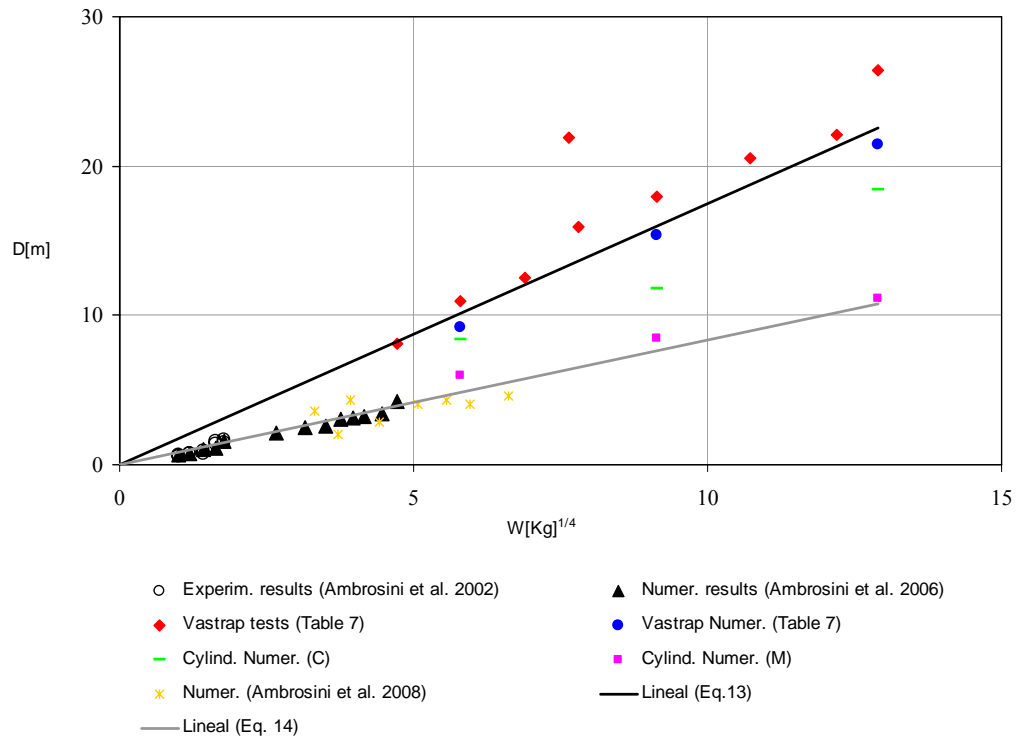
Figure 8: Proposed relationship for apparent crater diameter for explosive load on the ground.

6   BLAST WAVE PARAMETERS AND PLATE DEFLECTIONS

6.1 Introduction

In order to assess the parameters of the blast wave originated from different explosive layouts, the pressure and impulse time history at points situated at different distances from the explosive charge center were registered for all the cylindrical blast tests simulated. The gauge points were located at a height of 350mm in coincidence with the steel plates' centers in all cases.

6.2 Pressure

The resulting peak overpressure values as a function of the scaled distance are represented in Fig.10. Distances are measured from the explosive center. Some points corresponding to the numerical simulation of Vastrap tests 5 and 10 are also included in Fig.10. These points are coincident with some of the steel plates in the tests.

For the cases of cylindrical explosives, the same models were run but avoiding blast wave reflection on the ground and the corresponding results are also plotted on Figs.10. In this way, the effect of ground reflection can be evaluated. The effect of blast wave reflections on the ground is important in the case of compact explosives but it is almost negligible in case of widespread explosives.

The case of blast Test 1 but with cylindrical compact explosive was simulated with a finer mesh. Results corresponding to the refined mesh are almost coincident with those obtained with the coarser mesh used in the rest of the numerical models. This result proves that the refinement used is enough for this type of problems.

a)
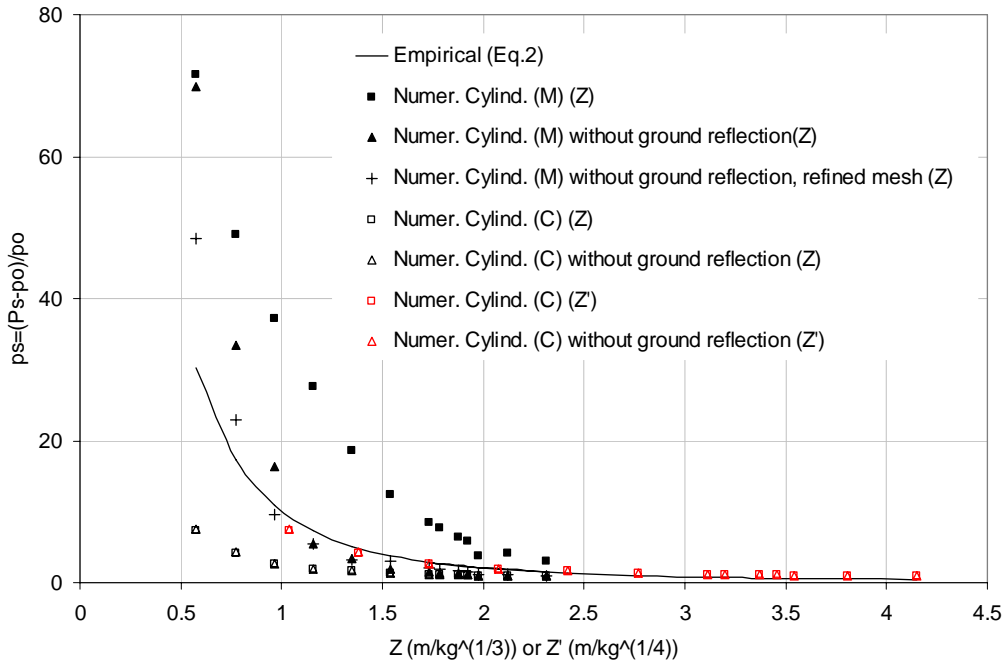
b)
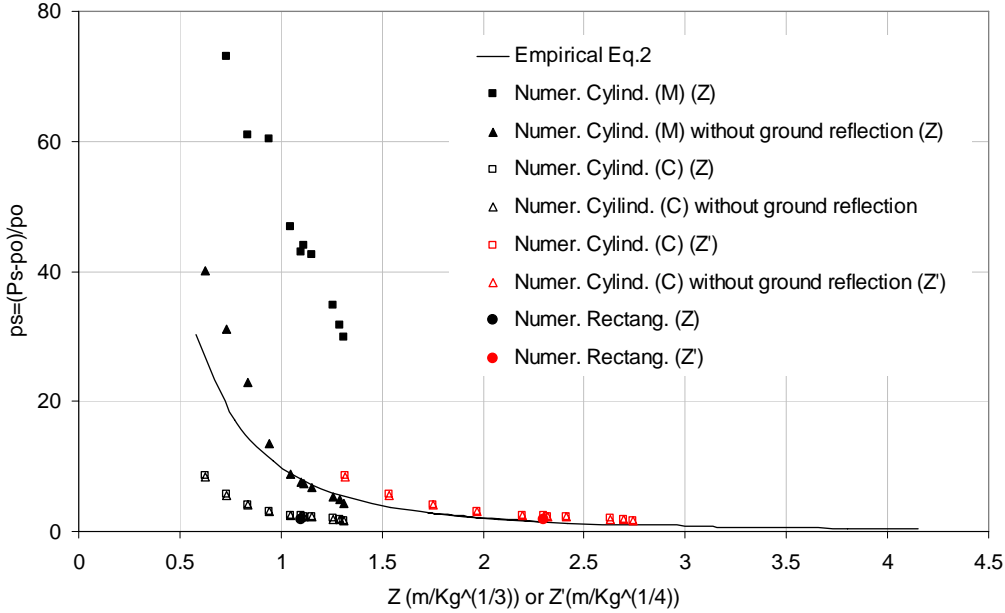
c)
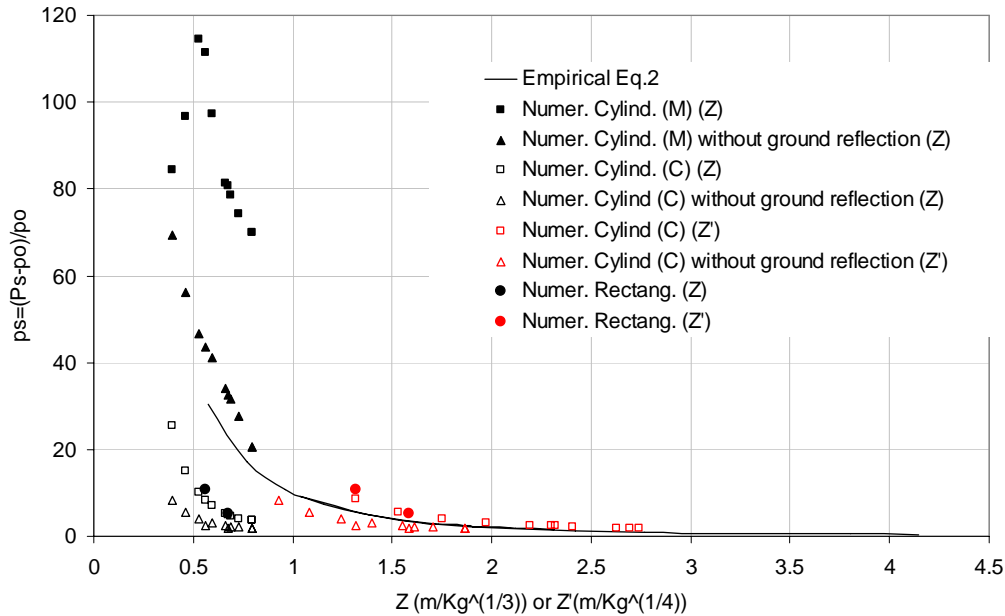
Figure 10: Peak side on overpressure vs scaled distance. a) Test 1 (1119.8 kg TNT); b) Test 5 (6945.4 kg TNT); c) Test 10 (27569.3 kg TNT)

The curves corresponding to empirical Eq.(2) are also included in Figs.10. The comparison with numerical results shows that while the cubic scale law works well for free field compact explosions, it is not appropriate for carpet like explosions. Following the results presented by Chung et al. (2008), a modified scaled distance is defined as

$$Z' = R / W^{1/4} \quad [\text{m/kg}^{1/4}] \tag{15}$$

Peak overpressure values obtained for the carpet like explosives are also represented as a function of Z' in Figs.10. The resulting points are almost coincident with the empirical curve corresponding to Eq.(2).

6.3 Impulse

The peak impulse values as a function of the scaled distance are represented in Fig.11. Like in the case of overpressure values, the impulse values for compact blast loads are greater than those for carpet like explosives. Nevertheless, the tendency of results is not so clear like in the case of overpressure values. Impulse values for compact explosive loads follow with some scattering the empiric curve presented by Kinney and Graham (1985). Points corresponding to impulse values are closer to that curve when they are represented as a function of the modified scaled distance Z' defined in Eq.(15) but they tend to a constant value, even greater than that predicted by empirical equations for high scaled distances ($Z' > 3$).

a)
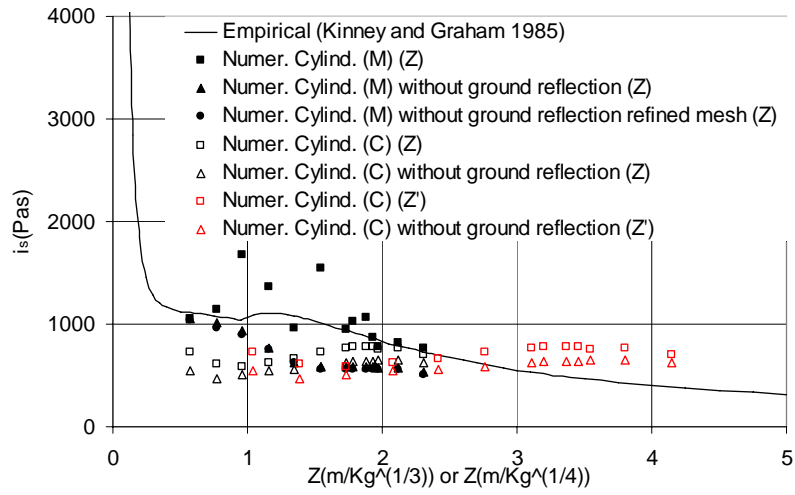
b)
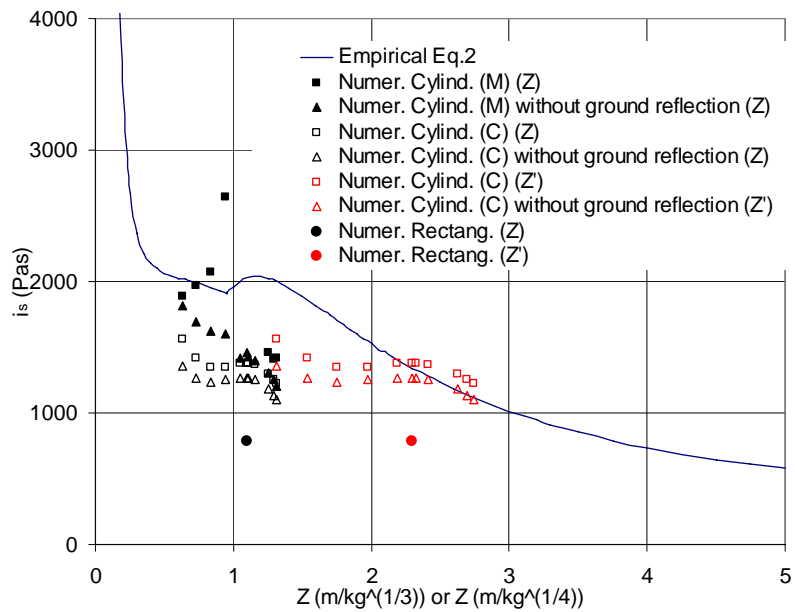
c)
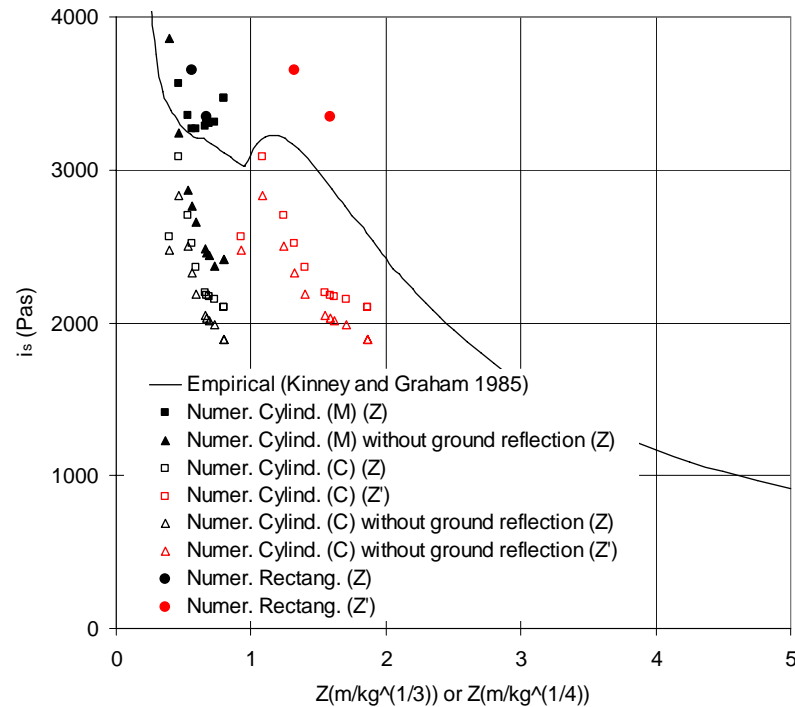
Figure 11. Peak side on impulse vs scaled distance. a) Test 1 (1119.8 kg TNT); b) Test 5 (6945.4 kg TNT); c) Test 10 (27569.3 kg TNT)

6.4 Plate deflections

With the impulse values empirically (Kinney and Graham, 1985) and numerically obtained, the plates deflections can be estimated using Eq.(3). Numerical values of impulse are directly obtained for the different models. Empirical values are calculated using the modified scaled distance Z'. The corresponding mid point deflection values are represented as a function of the measured mid point deflection in Fig.12.

In all cases, greater plate deflections are predicted for concentrated (M) than for carpet like explosives (C). Empirical results lie between those corresponding to the two types of explosive layout simulated: concentrated and spread. Although the points do not lie on the line representing the coincidence of evaluated and measured deflections, they are close to it. It seems that the use of Z' combined with Eq.(3) works better for smaller blast charges than for greater charges. Registered deflection is much greater than calculated values for greater charges.
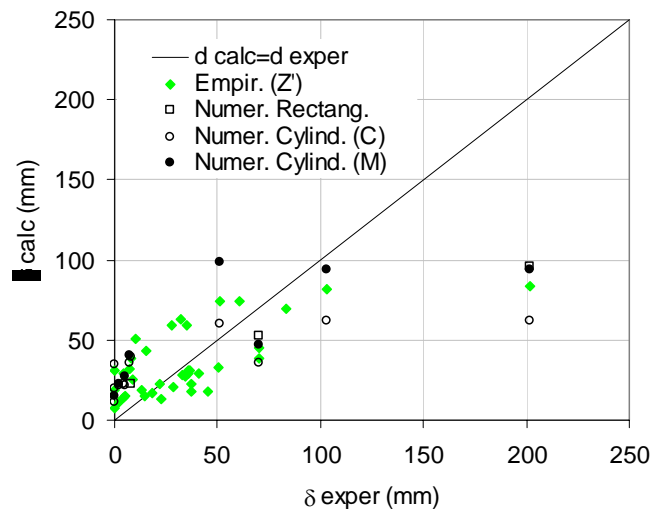
Figure 12. Plates mid point deflection

7   CONCLUSIONS

The numerical results presented in this paper provide an insight into the effect of large-scale explosions. The loading condition resulting from the detonation of large amount of ordnance widespread on the ground in a carpet like fashion has proven to be different to that originated from the detonation of compact explosives.

Reasonable agreement of numerical results with the experiment was obtained for crater dimensions. The shape and the dimensions of the crater formed in the underlying soil strongly depend on the explosive layout. The equivalent crater diameter for carpet like explosives is always grater than that for compact explosives. Moreover, for carpet like explosives, the equivalent diameter is greater for rectangular layouts than for circular layouts.

It was also proved that existing empirical formula for the prediction of crater diameter are not adequate for explosive masses greater than 3500 kg and new expressions covering all the range of explosives masses, from small to extreme cases, are proposed.

While the cube root scaled distance works well for evaluating the pressure and impulse values originated from a compact charge layout, the scaled distance parameter has to be modified to a fourth root for cases where charges are spread in a carpet-like fashion. The effect of blast wave reflections on the ground are almost negligible for this type of explosive layout.

8   AKNOWLEDGEMENTS

REFERENCES

Alia, A. and Souli, M., High explosive simulation using multi-material formulations. *Applied Thermal Engineering*, 26:1032–1042, 2006

Ambrosini, R.D., Luccioni, B., Danesi, R., Riera, J. and Rocha, M.. Size of Craters Produced by Explosive Charges on or Above the Ground Surface. *Shock Waves*, 12(1):69-78, 2002.

Ambrosini, R.D. and Luccioni, B. Craters produced by explosions on the soil surface. *Journal of Applied Mechanics, ASME*, 73(6):890-900, 2006

Ambrosini, D and Luccioni, B. Craters Produced by Large-Scale Explosions, Mecánica Computacional, XXVI:1801-1822, 2008

AUTODYN, *Explicit Software for Non-Linear Dynamics*, Version 11.0, User's Manual. Century Dynamics Inc, 2007.

Baker, W.E., Cox, P.A., Westine, P.S., Kulesz, JJ, Strehlow, RA. *Explosion hazards and evaluation*. Elsevier; 1983.

Chung Kim Yuen, S., Nurick, G.N., Verster, W. Jacob, N., Vara, A.R., Baldena, V.H. , Bwalya, D., Govender, R.A., Pittermann, R.A. Deformation of mild steel plates subjected to large-scale explosions. *International Journal of Impact Engineering,* 35:684–703, 2008.

Formby, S.A. and Wharton, R.K. Blast characteristics and TNT equivalence values for some commercial explosives detonated at ground level. *Journal of Hazardous Materials*, 50:183-198, 1996.

Guruprasad, S. and Mukherjee, A. Layered sacrificial claddings under blast loading Part II - experimental studies. *Int J Impact Eng,* 24(9):975-984, 2000.

Hanssen, A.G., Enstock, L, Langseth, M. Close-range blast loadin loading of aluminium foam panels. *International Journal of Impact Engineering*, 27(6):593–618, 2002.

Hirschfelder, J.O., Littler, D.J., and Sheard, H., Estimated blast pressures from TNT charges of 2 to 10000 tons, Los Alamos National Laboratory Library, LA Report 316, 3 9338 00350 4049:1-12., 1945.

Jacinto, A.C., Ambrosini, R.D., Danesi, R.F. Experimental and computational analysis of plates under air blast loading. *International Journal of Impact Engineering,* 25(10):927–47, 2001.

Kinney, G.F., Graham, K.J. *Explosive shocks in air*. 2nd ed. Springer Verlag; 1985.

Luccioni, B., Ambrosini D.and Danesi, R. Blast load assessment using Hydrocodes", *Engineering Structures* 28(12), (2006) 1736-1744.

Lee, E.L. and Tarver, C.M. Phenomenological model of shock initiation in heterogeneous explosives. *Physics of Fluids*, 23(12):2362-2372, 1980.

Lok, T.S. Response of solid circular ductile cantilever subjected to air-blast, Private communication, 2005.

Nurick, G.N., Martin, J.B. Deformation of thin plates subjected to impulsive loading—a review. Part I: Theoretical considerations. *International Journal of Impact Engineering*, 8(2):159–69, 1989a.

Nurick, G.N., Martin, J.B. Deformation of thin plates subjected to impulsive loading—a review. Part II: Experimental studies. *International Journal of Impact Engineering*, 8(2):171–86 1989b.

Nurick, G.N. and Shave, G.C. The deformation and tearing of thin square plates subjected to impulsive loads-an experimental study. *Int J Impact Eng,* 18(1):99-116, 1996.

Nurick, G.N., Chung Kim Yuen, S., Jacob, N., Verster, W., Bwalya, D.,Vara, A.R. Response of quadrangular mild-steel plates to large explosive load. *Second international conference on design analysis of protective structures (DAPS)*. Nanyang Technological University, 30–44, 2006.

Smith, P.D., Hetherington, J.G. *Blast and ballistic loading of structures*. Butterworth-Heinemann Ltd; 1994.

Teeling-Smith, R.G. and Nurick, G.N., The deformation and tearing of thin circular plates subjected to impulsive loads, *Int J Impact Eng,*11(1):77-91, 1991.

Wharton, R.K., Formby, S.A., and Merrifield, R. Airblast TNT equivalence for a range of commercial blasting explosives. *Journal of Hazardous Materials,* 79(1-2):31-39, 2000.